

Linking Axions, the Flavor Problem, and Neutrino Masses through a Flavored Peccei–Quinn Symmetry

Yithsbey Giraldo ^a and Eduardo Rojas ^b and Juan C. Salazar ^c

Departamento de Física, Universidad de Nariño, A.A. 1175, San Juan de Pasto, Colombia.

Received: date / Revised version: date

Abstract. Recent measurements by several experimental collaborations have reported deviations from Standard Model (SM) predictions in diphoton final states, potentially hinting at the existence of intermediate scalar resonances above the electroweak scale. Such anomalies can be naturally accommodated within SM extensions featuring an enlarged scalar sector. In particular, multi-Higgs doublet frameworks arise in Flavored Axion Models (FAMs), which have been proposed to explain the texture zeros of quark mass matrices. These models provide a unified description of quark masses and the Cabibbo–Kobayashi–Maskawa (CKM) mixing matrix while simultaneously addressing the strong CP problem. In this work we study a concrete FAM realization augmented with Majorana masses for right-handed neutrinos, implementing a type-I seesaw mechanism. In this model the flavor structure is effectively determined by the vacuum expectation values of the scalar doublets and Yukawa couplings of order one. Within this framework, neutrino and axion mass scales are intrinsically connected, as the heavy right-handed neutrinos obtain their masses from the scalar field responsible for the spontaneous breaking of the Peccei–Quinn symmetry. We further explore the phenomenological implications of the model, including constraints from flavor-changing neutral currents derived from semileptonic decays, as well as current experimental limits on the axion–photon coupling obtained from axion search experiments.

PACS. 11.30.Hv Flavor symmetries – 12.60.-i models beyond the standard models – 14.80.Va Axions – 14.60.St Non-standard-model particles Higgs bosons neutrinos – 14.80.-j Other particles (including hypothetical)

1 Introduction

The Peccei–Quinn (PQ) mechanism remains the most compelling resolution of the strong CP problem [1, 2]. By promoting CP to an effectively exact symmetry of QCD at low energies, the spontaneous breaking of a global $U(1)_{\text{PQ}}$ gives rise to a pseudo–Nambu–Goldstone boson—the axion—whose dynamics relax the QCD vacuum angle to zero [3, 4]. Concrete ultraviolet realizations such as the KSVZ and DFSZ frameworks embed the axion into extensions of the Standard Model (SM) with additional scalar fields and fermion charges [5, 6, 7, 8]. Comprehensive reviews of axion theory and phenomenology can be found in Refs. [9, 10].

Beyond solving strong CP, the PQ idea interfaces naturally with broader questions about the origin of mass scales in particle physics. Extended scalar sectors are a common ingredient in axion models (e.g. the DFSZ construction requires at least two Higgs doublets), opening

paths to address the electroweak hierarchy and to generate textures in the Yukawa matrices that account for the observed fermion mass hierarchies and mixings. In particular, identifying (or aligning) flavor symmetries with $U(1)_{\text{PQ}}$ can simultaneously control the axion couplings and reduce the number of free flavor parameters, yielding predictive textures for quarks and leptons [11, 12, 13, 14]. Recent work continues to develop “flavored” PQ scenarios and ν DFSZ variants that tie PQ breaking to the origin of neutrino masses and to controlled flavor structures [15, 16].

At the LHC, diboson final states are a sensitive probe of extended scalar sectors. A notable example is the rare SM decay $h \rightarrow Z\gamma$, where the ATLAS and CMS combination finds first evidence with a signal strength modestly above the SM expectation, albeit with current uncertainties [17]. Such loop–induced channels, together with precision measurements of $h \rightarrow \gamma\gamma$, constrain additional charged states and nonstandard scalar mixing. In parallel, direct searches for neutral resonances decaying to $\gamma\gamma$ or $Z\gamma$ have set stringent limits across a wide mass range [18, 19, 20, 21]. While no conclusive excess has emerged, several analyses report mild, localized deviations that motivate scalar explanations consistent with current bounds,

Send offprint requests to:

^a yithsbey@gmail.com

^b eduro4000@gmail.com

^c jusala@gmail.com

especially in models predicting enhanced loop couplings to photons and $Z\gamma$.

These considerations motivate the class of models we study here: an extended scalar sector with several $SU(2)_L$ doublets and two singlets, organized by a flavored PQ symmetry. The presence of multiple Higgs doublets is not only natural in axion frameworks (as in DFSZ) but, when combined with appropriate PQ charge assignments, can generate realistic Yukawa textures through symmetry selection rules. The same doublets contain additional charged and neutral scalar states that can modify the loop-induced diboson rates, potentially accounting for hints in $Z\gamma$ and $\gamma\gamma$ while remaining compatible with existing collider limits. In general, constraints on the axion-photon coupling require the axion to be light, which in turn implies the presence of at least one scalar field acquiring a vacuum expectation value (VEV) of order 10^6 GeV. Since several scalar couplings are unavoidable, this large VEV can raise the masses of the scalar states above the TeV scale, making the model incompatible with the Higgs-like resonances we aim to analyze, which typically appear at a few hundred GeV. We find, however, that by appropriately choosing the trilinear terms in the scalar potential (dimension-three interactions involving only scalar fields), a phenomenologically viable scenario can be achieved.

Our analysis will delineate the parameter space where the axion solution to strong CP, flavor textures, and diboson phenomenology are simultaneously realized.

The manuscript is organized as follows. In Sec. 2 we review the quark and lepton mass-matrix textures employed throughout this work and express their real parameters in terms of the Standard Model fermion masses and two additional free parameters. In Sec. 3 we introduce the particle content of the model and specify the Peccei-Quinn charge assignments required to reproduce the mass textures discussed in Sec. 2.

In Sec. 4 we determine the Yukawa couplings consistent with the observed charged-lepton and neutrino masses. Sec. 5 is devoted to the scalar sector: we construct the most general scalar potential compatible with the symmetries of the model and perform a numerical scan of the parameter space to identify the regions yielding scalar-boson mass spectra consistent with the proposed diphoton excesses.

In Sec. 6 we analyze the relation between the neutrino and axion mass scales. In Sec. 7 we derive the relevant low-energy constraints. Finally, Sec. 8 summarizes our results and presents our conclusions.

2 The Five texture-zero mass matrices

The motivation behind considering texture zeros in the Standard Model (SM) and its extensions is to reduce the number of independent parameters, thereby revealing potential correlations between masses and mixings in these models. The Yukawa Lagrangian provides the mechanism for fermion mass generation after spontaneous symmetry breaking. One initial simplification, without loss of generality, is to assume that the fermion mass matrices are

Hermitian, which brings the number of free parameters in each quark and lepton sector down to 18. However, even with this reduction, there are still more parameters than needed to match the experimental data available in the literature. Since no comprehensive model exists to make accurate predictions, discrete symmetries are often employed to eliminate certain elements from the Yukawa matrix, resulting in texture zeros. In numerous studies, instead of introducing discrete symmetries, texture zeros are proposed as a more straightforward and practical alternative. This approach offers the advantage of allowing the selection of mass matrices in a way that optimizes the analytical treatment of the problem, while simultaneously enabling adjustments to the fermion masses and mixing angles.

2.1 A Realistic Texture for Quark Mass Matrices

It is important to note that six-zero textures in the Standard Model have already been ruled out, as their predictions fall outside the experimentally allowed ranges. However, five-zero textures for quark mass matrices remain a plausible option [22, 23, 24, 25, 26, 27]. In particular, we focus on selecting five-zero textures that align well with the observed quark masses and mixing parameters, as demonstrated in previous works [28, 29, 30].

$$M^U = \begin{pmatrix} 0 & 0 & C_u \\ 0 & A_u & B_u \\ C_u^* & B_u^* & D_u \end{pmatrix}, \quad (1)$$

$$M^D = \begin{pmatrix} 0 & C_d & 0 \\ C_d^* & 0 & B_d \\ 0 & B_d^* & A_d \end{pmatrix}.$$

The phases in M^D can be removed by applying a weak basis transformation (WBT) [28, 31, 32], which shifts these phases to the off-diagonal components of M^U . This procedure enables the mass matrices in equation (1) to be expressed in an alternative form:

$$M^U = \begin{pmatrix} 0 & 0 & |C_u|e^{i\phi_{C_u}} \\ 0 & A_u & |B_u|e^{i\phi_{B_u}} \\ |C_u|e^{-i\phi_{C_u}} & |B_u|e^{-i\phi_{B_u}} & D_u \end{pmatrix}, \quad (2)$$

$$M^D = \begin{pmatrix} 0 & |C_d| & 0 \\ |C_d| & 0 & |B_d| \\ 0 & |B_d| & A_d \end{pmatrix},$$

By utilizing the trace and determinant of the mass matrices (2), both prior to and following the diagonalization procedure, the independent real parameters of M^U and M^D can be expressed in terms of their corresponding

masses:

$$D_u = m_u - m_c + m_t - A_u, \quad (3a)$$

$$|B_u| = \sqrt{\frac{(A_u - m_u)(A_u + m_c)(m_t - A_u)}{A_u}}, \quad (3b)$$

$$|C_u| = \sqrt{\frac{m_u m_c m_t}{A_u}}, \quad (3c)$$

$$A_d = m_d - m_s + m_b, \quad (3d)$$

$$|B_d| = \sqrt{\frac{(m_b - m_s)(m_d + m_b)(m_s - m_d)}{m_d - m_s + m_b}}, \quad (3e)$$

$$|C_d| = \sqrt{\frac{m_d m_s m_b}{m_d - m_s + m_b}}. \quad (3f)$$

One effective approach is to assume that the masses of the second-generation quarks are negative, corresponding to eigenvalues of $-m_c$ and $-m_s$. The parameter A_u remains free, and its value, which is set by the quark mass hierarchy, must fall within the specified range:

$$m_u \leq A_u \leq m_t. \quad (4)$$

The detailed step-by-step method for diagonalizing the mass matrices (2) is outlined in Appendix C reference [33].

3 PQ symmetry and the minimal particle content

3.1 Yukawa Lagrangian and the PQ symmetry

The texture-zeros of the mass matrices presented in equations (2) can be produced by applying a Peccei-Queen symmetry, $U(1)_{PQ}$, to the Lagrangian model as shown in Eq.(5)[13,34,35]. As elaborated upon below, the minimal Lagrangian necessary to incorporate this symmetry is described in [33,36].

$$\begin{aligned} \mathcal{L}_{\text{LO}} \supset & (D_\mu \Phi^\alpha)^\dagger D^\mu \Phi^\alpha + \sum_\psi i \bar{\psi} \gamma^\mu D_\mu \psi + \sum_{i=1}^2 (D_\mu S_i)^\dagger D^\mu S_i \\ & - \left(\bar{q}_{Li} y_{ij}^{D\alpha} \Phi^\alpha d_{Rj} + \bar{q}_{Li} y_{ij}^{U\alpha} \tilde{\Phi}^\alpha u_{Rj} \right. \\ & \left. + \bar{\ell}_{Li} y_{ij}^E \Phi_3 e_{Rj} + \bar{\ell}_{Li} y_{ij}^\nu \tilde{\Phi}_3 \nu_{Rj} + \frac{1}{2} Y_{ij}^N \bar{\nu}_{Ri} \nu_{Rj} S_2^\dagger + \text{h.c.} \right) \\ & + (\lambda_Q \bar{Q}_R Q_L S_2 + \text{h.c.}) - V(\Phi, S_1, S_2). \end{aligned} \quad (5)$$

As demonstrated in reference [33], the generation of quark mass textures necessitates the presence of at least four Higgs doublets, denoted as $\alpha = 1, 2, 3, 4$.

In the context of (5), the indices i and j represent families (with an implied summation over any repeated indices). The superscripts U , D , E , and N correspond to the up-type quarks, down-type quarks, electron-like fermions, and neutrino-like fermions, respectively. The covariant derivative in the Standard Model is given by $D_\mu = \partial_\mu + iF_\mu^{\text{SM}}$.

The charged leptons and neutrinos carry universal Peccei-Quinn charges and couple through Yukawa interactions to the scalar doublet Φ_3 . The right-handed neutrinos acquire Majorana masses, allowing the implementation of a Type-I seesaw mechanism. In an earlier work [37], we considered texture-zero structures for the lepton masses; however, this approach proved unnatural in the lepton sector. In the present model, we instead adopt the conventional Type-I seesaw solution to account for the smallness of neutrino masses.

For details on the scalar potential $V(\Phi, S_1, S_2)$, refer to Section 5 and to the comprehensive information in reference [33]. In Eq.(5), ψ denotes the set of Standard Model fermion fields along with the heavy quark Q , which are identified in Tables 1 and 2.

As illustrated in Table 2, the PQ charges for the heavy quark can be configured to permit interactions exclusively with the scalar singlet S_2 .

The Q_{PQ} charges are assigned as follows: for left-handed quark doublets (q_L), we use x_{q_i} ; for right-handed up-type quark singlets (u_R), x_{u_i} ; for right-handed down-type quark singlets (d_R), x_{d_i} ; for left-handed lepton doublets (ℓ_L), x_{ℓ_i} ; for right-handed charged leptons (e_R), x_{e_i} ; and for right-handed Dirac neutrinos (ν_R), x_{ν_i} for each family ($i = 1, 2, 3$). A similar notation applies to the scalar doublets, x_{ϕ_α} ($\alpha = 1, 2, 3, 4$), as well as the scalar singlets $x_{S_{1,2}}$.

Particles	Spin	$SU(3)_C$	$SU(2)_L$	$U(1)_Y$	$U_{PQ}(i=1)$	$U_{PQ}(i=2)$	$U_{PQ}(i=3)$	Q_{PQ}
q_{Li}	1/2	3	2	1/6	$-2s_1 + 2s_2 + \alpha_q$	$-s_1 + s_2 + \alpha_q$	α_q	x_{q_i}
u_{Ri}	1/2	3	1	2/3	$s_1 + \alpha_q$	$s_2 + \alpha_q$	$-s_1 + 2s_2 + \alpha_q$	x_{u_i}
d_{Ri}	1/2	3	1	-1/3	$2s_1 - 3s_2 + \alpha_q$	$s_1 - 2s_2 + \alpha_q$	$-s_2 + \alpha_q$	x_{d_i}
ℓ_{Li}	1/2	1	2	-1/2	$\frac{x_{QR} - x_{QL}}{2} + s_1 - 2s_2$	$\frac{x_{QR} - x_{QL}}{2} + s_1 - 2s_2$	$\frac{x_{QR} - x_{QL}}{2} + s_1 - 2s_2$	x_{ℓ_i}
e_{Ri}	1/2	1	1	-1	$\frac{x_{QR} - x_{QL}}{2} + 2s_1 - 4s_2$	$\frac{x_{QR} - x_{QL}}{2} + 2s_1 - 4s_2$	$\frac{x_{QR} - x_{QL}}{2} + 2s_1 - 4s_2$	x_{e_i}
ν_{Ri}	1/2	1	1	0	$\frac{x_{QR} - x_{QL}}{2}$	$\frac{x_{QR} - x_{QL}}{2}$	$\frac{x_{QR} - x_{QL}}{2}$	x_{ν_i}

Table 1. Particle content. The subindex $i = 1, 2, 3$ stand for the family number in the interaction basis. Columns 6-8 are the Peccei-Quinn charges, Q_{PQ} , for each family of quarks and leptons in the SM. s_1, s_2 and α are real parameters, with $s_1 \neq s_2$.

Particles	Spin	$SU(3)_C$	$SU(2)_L$	$U(1)_Y$	U_{PQ}	Q_{PQ}
Φ_1	0	1	2	1/2	s_1	x_{ϕ_1}
Φ_2	0	1	2	1/2	s_2	x_{ϕ_2}
Φ_3	0	1	2	1/2	$-s_1 + 2s_2$	x_{ϕ_3}
Φ_4	0	1	2	1/2	$-3s_1 + 4s_2$	x_{ϕ_4}
Q_L	1/2	3	1	0	x_{Q_L}	x_{Q_L}
Q_R	1/2	3	1	0	x_{Q_R}	x_{Q_R}
S_1	0	1	1	0	$s_1 - s_2$	x_{s_1}
S_2	0	1	1	0	$x_{Q_R} - x_{Q_L}$	x_{s_2}

Table 2. Beyond the SM fields and their respective PQ charges. The parameters s_1, s_2 are reals, with $s_1 \neq s_2$ and $x_{Q_R} \neq x_{Q_L}$.

In this study, the PQ charges attributed to both the quark and scalar sectors, along with the VEVs assigned to the scalar doublets, will mirror those assigned in [33], as detailed in Tables(1) and (2).

Our model incorporates two scalar singlets, S_1 and S_2 , responsible for breaking the global symmetry $U(1)_{PQ}$.

The QCD anomaly associated with the PQ charges is described by:

$$N = 2 \sum_{i=1}^3 x_{q_i} - \sum_{i=1}^3 x_{u_i} - \sum_{i=1}^3 x_{d_i} + A_Q, \quad (6)$$

where $A_Q = x_{Q_L} - x_{Q_R}$ accounts for the anomaly contribution from the heavy quark Q , which is an electroweak gauge group singlet. The left and right Peccei-Quinn charges are denoted by x_{Q_L} and x_{Q_R} , respectively.

We express these charges as a function of N , ensuring that N is non-zero, such that

$$s_1 = \frac{N}{9} \hat{s}_1, \quad s_2 = \frac{N}{9} (\epsilon + \hat{s}_1), \quad \text{with} \quad \epsilon = 1 - \frac{A_Q}{N}, \quad (7)$$

where \hat{s}_1 and ϵ are arbitrary real values.

To address the strong CP problem with $N \neq 0$ while also generating texture-zeros in the mass matrices, it is essential to ensure $\epsilon = \frac{9(s_2 - s_1)}{N} \neq 0$.

In this context, concerning Flavor-Changing Neutral Currents (FCNC) observables, the parameters of interest are \hat{s}_1 and ϵ .

This parameterization proves particularly useful, especially when the parameters α_q and α_ℓ are not significant, because by setting N and f_a , we can adjust \hat{s}_1 and ϵ while keeping $\Delta_{PQ} = f_a N$ constant. This allows the parameter space to be effectively reduced to two dimensions.

4 Naturalness of Yukawa couplings

As demonstrated in Ref. [33], the realization of five texture zeros in the quark mass matrices of Eq. (1), enforced by a Peccei-Quinn (PQ) symmetry, requires the introduction

of at least four scalar $SU(2)_L$ doublets. Once the electroweak symmetry is spontaneously broken, the up- and down-type quark mass matrices can be written as

$$M^U = \hat{v}_\alpha y_{ij}^{U\alpha} = \begin{pmatrix} 0 & 0 & y_{13}^{U1} \hat{v}_1 \\ 0 & y_{22}^{U1} \hat{v}_1 & y_{23}^{U2} \hat{v}_2 \\ y_{13}^{U1*} \hat{v}_1 & y_{23}^{U2*} \hat{v}_2 & y_{33}^{U3} \hat{v}_3 \end{pmatrix},$$

$$M^D = \hat{v}_\alpha y_{ij}^{D\alpha} = \begin{pmatrix} 0 & |y_{12}^{D4}| \hat{v}_4 & 0 \\ |y_{12}^{D4}| \hat{v}_4 & 0 & |y_{23}^{D3}| \hat{v}_3 \\ 0 & |y_{23}^{D3}| \hat{v}_3 & y_{33}^{D2} \hat{v}_2 \end{pmatrix}, \quad (8)$$

where $\hat{v}_i \equiv v_i/\sqrt{2}$ are defined in terms of the vacuum expectation values of the scalar doublets.

It was further shown in Ref. [33] that the five-zero textures of Eq. (2) allow most of the quark Yukawa couplings to be naturally of order unity, with the exception of y_{23}^{U2} , y_{23}^{D3} , and y_{13}^{U1} . Under this assumption, one obtains

$$\hat{v}_1 = 1.71 \text{ GeV}, \quad \hat{v}_2 = 2.91 \text{ GeV},$$

$$\hat{v}_3 = 174.085 \text{ GeV}, \quad \hat{v}_4 = 13.3 \text{ MeV}. \quad (9)$$

Although hermiticity is not automatically guaranteed in a generic multi-Higgs framework [38], it is well motivated to impose it in the present context. First, in the Standard Model and in many of its extensions where right-handed fermions are $SU(2)_L$ singlets, the quark mass matrices can be chosen Hermitian without loss of generality. Second, this property remains valid even after implementing an additional PQ symmetry. Third, Hermitian textures permit the application of the weak-basis transformation (WBT) method [28]. Finally, there exists an extensive body of phenomenologically viable Hermitian quark mass matrices in the literature. We emphasize that the mass matrices given in Eq. (8) satisfy the Hermiticity condition.

5 Scalar potential

The scalar sector under consideration includes four Higgs doublets ($\Phi_{1,2,3,4}$) and two complex scalar singlets ($S_{1,2}$), embedded into the broader program of Higgs-like resonance searches at the LHC. The resulting spectrum—six CP-even, three CP-odd, and six charged scalars—offers a consistent interpretation of the 95 GeV diphoton excess, the Standard-Model-like Higgs at 125 GeV, and possible

heavier scalar states extending up to the multi–TeV scale. Relevant decay modes, current collider constraints, and flavour observables have been analysed, with projections for LHC Run 3 and the HL–LHC also taken into account.

Motivated by multi–Higgs models with a global Peccei–Quinn (PQ) symmetry aimed at solving the strong–CP problem [1], the setup assumes an extended scalar sector preserving $SU(2)_L \times U(1)_Y \times U(1)_{\text{PQ}}$, where all doublets carry SM quantum numbers. The scalar fields are written as

$$\begin{aligned} \Phi_\alpha &= \begin{pmatrix} \phi_\alpha^+ \\ v_\alpha + h_\alpha + i\eta_\alpha \\ \sqrt{2} \end{pmatrix}, & \tilde{\Phi}_\alpha &= i\sigma_2 \Phi_\alpha^*, & \alpha &= 1, 2, 3, 4, \\ S_i &= \frac{v_{s_i} + \xi_{s_i} + i\zeta_{s_i}}{\sqrt{2}}; & & & i &= 1, 2, \end{aligned} \quad (10)$$

with vacuum expectation values satisfying the hierarchy $v_4 \ll v_1, v_2 \ll v_3 \ll v_{s_2}$, as previously established in [33, 37]. These VEVs, along with suitable PQ charge assignments, induce Yukawa textures with predictive power in the quark sector, reproducing observed masses and CKM mixing while suppressing the number of free parameters. A vector–like quark, charged under PQ symmetry, acquires mass through the coupling $\mathcal{L} \supset \lambda_Q S_2 \bar{Q}_L Q_R + \text{h.c.}$, which ensures the finiteness of QCD–PQ anomalies and helps control FCNC effects.

The singlet S_2 breaks the PQ symmetry at a high scale, $f_a^2 = \sum_i (x_i v_i)^2 \approx x_{s_2}^2 v_{s_2}^2 \approx (10^{15})^2 \text{ GeV}^2$ (see Appendix B). However, in contrast with earlier implementations [33, 37], and despite the large value of v_{s_2} , it is possible to obtain a spectrum for scalar masses in the range of 100 GeV, as suggested by the Higgs–like signatures observed at the LHC, as shown in the figure 1. A numerical scan over v_{s_1} in the range 50 GeV– 40×10^3 GeV revealed that beyond this range, it becomes increasingly difficult to obtain scalar masses below 1 TeV. Due to the large value of v_{s_2} , the model predicts a light axion state. Since the axion decay constant scales as $f_a \propto v_{s_2}$, the axion mass behaves as $m_a = (7.5 \times 10^{-2} \text{ GeV})^2 / f_a$, leading to a suppressed axion mass for sizable v_{s_2} .

The scalar potential compatible with the symmetries includes quadratic, quartic, and specific trilinear interac-

tions:

$$\begin{aligned} V(\Phi_i, S_j) &= \sum_{i=1}^4 \mu_i^2 \Phi_i^\dagger \Phi_i + \sum_{k=1}^2 \mu_{s_k}^2 S_k^* S_k + \sum_{i=1}^4 \lambda_i (\Phi_i^\dagger \Phi_i)^2 \\ &+ \sum_{k=1}^2 \lambda_{s_k} (S_k^* S_k)^2 + \sum_{i=1}^4 \sum_{k=1}^2 \lambda_{i s_k} (\Phi_i^\dagger \Phi_i) (S_k^* S_k) \\ &+ \underbrace{\sum_{i,j=1}^4}_{i < j} \left(\lambda_{ij} (\Phi_i^\dagger \Phi_i) (\Phi_j^\dagger \Phi_j) + J_{ij} (\Phi_i^\dagger \Phi_j) (\Phi_j^\dagger \Phi_i) \right) \\ &+ \lambda_{s_1 s_2} (S_1^* S_1) (S_2^* S_2) + K_1 \left((\Phi_1^\dagger \Phi_2) (\Phi_3^\dagger \Phi_2) + \text{h.c.} \right) \\ &+ K_2 \left((\Phi_3^\dagger \Phi_4) (\Phi_3^\dagger \Phi_1) + \text{h.c.} \right) \\ &+ K_3 \left((\Phi_3^\dagger \Phi_4) S_1^2 + \text{h.c.} \right) + K_4 \left((\Phi_1^\dagger \Phi_3) S_1^2 + \text{h.c.} \right) \\ &+ F_1 \left((\Phi_2^\dagger \Phi_3) S_1 + \text{h.c.} \right) + F_2 \left((\Phi_1^\dagger \Phi_2) S_1 + \text{h.c.} \right) \\ &+ \frac{1}{2} (m_{\zeta_{s_2}})_{\text{SB}}^2 \zeta_{s_2}^2 + \frac{1}{2} (m_{\xi_{s_2}})_{\text{SB}}^2 \xi_{s_2}^2. \end{aligned} \quad (11)$$

Due to its PQ charge, S_2 does not couple trilinearly or quartically to the doublets, while S_1 does. The F_i couplings arise from the PQ charge assignments and have mass dimension one. The singlet S_2 also provides mass to the heavy quark Q .

To preserve naturalness, the following dimensionless parameters in the potential (11) were chosen in the range:

$$\lambda_{i s_k}, \lambda_{ij}, J_{ij}, \lambda_{s_1 s_2}, K_1, K_2, K_4 \in [-1.5, 1.5]. \quad (12)$$

Additionally, to ensure the scalar potential is stable—i.e., bounded from below—its stability is determined solely by the quartic terms in V:

$$\lambda_i, \lambda_{s_k} \in [0, 1.5]. \quad (13)$$

Despite being dimensionless, K_3 is subject to stronger constraints, leading to narrower intervals. Similar considerations apply to F_1 and F_2 :

$$\begin{aligned} F_1 &\in [-45, 10] \text{ GeV}, \\ F_2 &\in [-600, 600] \text{ GeV}, \\ K_3 &\in [-1.5, 0.2]. \end{aligned} \quad (14)$$

After electroweak symmetry breaking, one neutral CP–odd Goldstone G^0 and one charged Goldstone pair G^\pm are absorbed by Z and W^\pm , respectively. The remaining neutral CP–odd massless state is the axion a , the (pseudo–)Nambu–Goldstone boson associated with the spontaneous breaking of $U(1)_{\text{PQ}}$. The physical spectrum then comprises six CP–even scalars $H_{1\dots 6}$, four CP–odd states $\{A_1, A_2, A_3, a\}$, and three charged scalar pairs $C_{1\dots 3}^\pm$.

We define the real orthogonal matrix R that diagonalizes the CP–even mass matrix in the gauge basis

$$\Phi = (h_1, h_2, h_3, h_4, \xi_{s_1}, \xi_{s_2}) : R^T M_H^2 R = \text{diag}(m_{H_1}^2, \dots, m_{H_6}^2).$$

The entry $R_{ik} \equiv \langle \Phi_i | H_k \rangle$ quantifies the admixture of Φ_i in H_k .

For the hierarchy $v_{s_2} \gg v_{s_1} \gtrsim v_3 \gg v_{1,2} \gg v_4$, the states $H_6 \simeq S_2$ and $H_5 \simeq \Phi_4$ naturally decouple. The former does so because $m_{H_6}^2 \simeq 2\lambda_{s_2}v_{s_2}^2$, while the latter becomes heavy since $(M_H^2)_{44} \approx \frac{v_3}{2v_4}(K_2v_1v_3 + K_3v_{s_1}^2)$, except for the unlikely case of a fine-tuned cancellation, $K_2v_1v_3 + K_3v_{s_1}^2 \simeq 0$, the entry $(M_H^2)_{44}$ remains large. If such a cancellation were to occur, $(M_H^2)_{44}$ would be suppressed and the mixing significantly enhanced; this corresponds to a tuned region of parameter space. The mode

H_2 aligns with the SM Higgs boson, $H_2 \approx \Phi_3$, with tiny admixtures (corresponding to $|R_{32}| \rightarrow 1$), thereby reproducing the measured SM Higgs couplings. In contrast, the light state $H_1 \simeq 95$ GeV originates from the subspace spanned by h_1 and h_2 , orthogonal to the direction associated with h_3 . This state can contain at most a small component $|R_{31}| = |\langle \Phi_3 | H_1 \rangle| \lesssim 0.243$, which is sufficient to reproduce the $\gamma\gamma$ signal strength without placing the SM Higgs couplings under tension.

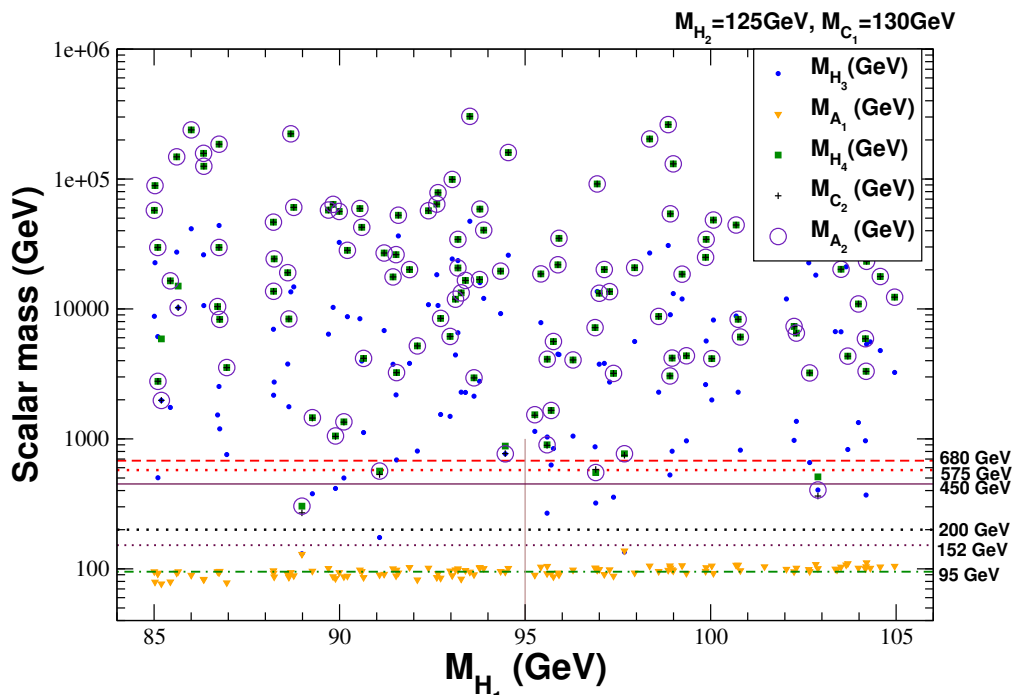


Fig. 1. To connect with current phenomenology we set $M_{H_1} = 95$ GeV, $M_{H_2} = 125$ GeV, $M_{C_1} = 130$ GeV. Heavier scalars span the ranges $M_{H_3} \in [200 \text{ GeV}, 50 \text{ TeV}]$, $M_{C_2} \in [300 \text{ GeV}, 300 \text{ TeV}]$, $M_{A_1} \in [95 \text{ GeV}, 150 \text{ GeV}]$. Higher states are taken above the current LHC reach.

The diphoton signature near 95 GeV is mediated by the light CP-even state H_1 . Its effective coupling to photons is loop-induced by charged fermions and is further controlled by the small component of H_1 along the SM-like direction Φ_3 . In our benchmark, this overlap is quantified by $R_{31} \equiv \langle \Phi_3 | H_1 \rangle$. The next-to-lightest state H_2 is aligned with the SM Higgs direction and accounts for the observed 125 GeV signal.

From a broader perspective, most recent interpretations of the $\gamma\gamma$ feature around $m_{\gamma\gamma} \simeq 95$ GeV embed the putative resonance in minimal extensions of the Two-Higgs-Doublet Model. A common strategy is to supplement the 2HDM with an additional gauge-singlet (pseudo) scalar (sometimes with a second singlet), or to introduce an inert sector, so that the neutral spectrum contains mass eigenstates that are admixtures of singlet and dou-

blet fields. In many such constructions a (softly-broken) \mathbb{Z}_2 symmetry is imposed to enforce natural flavour conservation and suppress tree-level FCNCs in the Yukawa sector, while in other scenarios this role is replaced or complemented by a gauged $U(1)'$ symmetry (e.g. $U(1)_H$ or flavour-dependent $U(1)_X$), which further restricts the scalar potential and Yukawa structure and may require extra chiral matter for anomaly cancellation [39, 40, 41, 42, 43, 44, 45, 46]. Complementary studies show that diphoton anomalies—including the 95 GeV structure—can also be accommodated within 2HDM frameworks without additional singlet scalars, for instance in aligned and phenomenologically constrained setups where the light state remains predominantly doublet-like [47, 48, 49].

In the present work, the enlarged scalar sector is not introduced ad hoc to fit the excess: it is dictated by the

Peccei–Quinn charge assignments required by the flavored-axion construction and by the texture structure of the quark Yukawa matrices. In this setting, the suppression of tree-level FCNCs follows from the same PQ-driven Yukawa pattern together with the hierarchy $v_{1,2,4} \ll v_3$, rather than from imposing a \mathbb{Z}_2 symmetry. The complex singlets $S_{1,2}$ primarily implement PQ breaking and (as discussed in the next section) generate the Majorana masses of right-handed neutrinos, while the collider phenomenology of the 95 GeV state is governed dominantly by the doublet sector and its controlled admixture with Φ_3 .

6 Axion–Neutrino Mass Relation

In our model, after spontaneous symmetry breaking, the Yukawa interaction that generates the neutrino mass is given by

$$-\mathcal{L}_{Y\nu} = y_{ij}^\nu \frac{v_{SM}}{\sqrt{2}} \bar{\nu}_{Li} \nu_{Rj} + \frac{1}{2} Y_{ij}^N \bar{\nu}_{Ri}^c \nu_{Rj} \frac{v_{s_2}}{\sqrt{2}} + \text{h.c.} \quad (15)$$

induces Majorana masses for the right-handed neutrinos once the scalar field S_2 acquires a vacuum expectation value (VEV), v_{s_2} . Consequently, the right-handed neutrino mass matrix is given by $m_{ij}^N = \frac{1}{\sqrt{2}} Y_{ij}^N v_{s_2}$. In a similar way the Dirac neutrino mass matrix is $m_{ij}^D = Y_{ij}^\nu v_{SM}/\sqrt{2}$, where $v_{\Phi_3} \sim v_{SM} \sim 246\text{GeV}$, in such a way that the left-handed neutrinos mass matrix is

$$m_{ij}^\nu = - (m_D m_N^{-1} m_D)_{ij} = - \frac{v_{SM}^2}{\sqrt{2} v_{s_2}} (Y^\nu Y_N^{-1} Y^\nu)_{ij} \quad (16)$$

At the same time, as discussed in the previous section, the axion decay constant is given by $f_a \simeq v_{s_2} x_{s_2}$. From (34) $m_a = (7.55 \times 10^{-2} \text{GeV})^2 / f_a \simeq \frac{(7.55 \times 10^{-2} \text{GeV})^2}{x_{s_2} v_{s_2}}$, in such a way that the neutrino mass matrix is proportional to the axion mass, i.e., $m_{ij}^\nu = -x_{s_2} (Y^\nu Y_N^{-1} Y^\nu)_{ij} \times 7.5 \times 10^6 m_a$. In the standard model $(Y^\nu)^2$ ranges from $\sim 10^{-11}$ for the electron to 1 for the top quark, which implies a wide range for the axion masses. The neutrino mass matrix must be less than the cosmological bound (i.e., $\sum_i m_{\nu_i} \leq 0.12\text{eV}$), which implies $|x_{s_2} \text{Tr}(Y^\nu Y_N^{-1} Y^\nu) \times 10^6 m_a| \leq 0.12\text{eV}$. On the other hand, the trace of the neutrino mass determinant is the product of the three neutrino masses, i.e., $m_1^\nu m_2^\nu m_3^\nu = - \frac{(\det Y^\nu)^2}{\det Y^N} (x_{s_2} 7.5 \times 10^6 m_a)^3$. Combining the neutrino oscillation data and the cosmological upper bound on the neutrino masses it is possible to bound the neutrino mass determinant $\det(m^\nu) = m_1^\nu m_2^\nu m_3^\nu$,

$$0 \leq |m_1^\nu m_2^\nu m_3^\nu| \leq \begin{cases} (0.038\text{eV})^3, & \text{N.O.} \\ (0.034\text{eV})^3, & \text{I.O.} \end{cases}, \quad (17)$$

which implies

$$\left| x_{s_2} \frac{(\det Y^\nu)^{2/3}}{(\det Y^N)^{1/3}} \right| m_a \leq \begin{cases} 5.1 \times 10^{-9} \text{eV}, & \text{N.O.} \\ 4.5 \times 10^{-9} \text{eV}, & \text{I.O.} \end{cases} \quad (18)$$

7 Low energy constraints

7.1 Flavor changing neutral currents

Since our setup involves non-universal PQ charges, a tree-level assessment of flavor-changing neutral currents (FCNCs) is required in addition to the standard bounds on the axion–photon coupling. As emphasized in Ref. [10], the most stringent limits on axion–quark flavor-violating interactions arise from meson decays into invisible final states. At present, the process $K^\pm \rightarrow \pi^\pm a$ provides the leading constraints on the axion mass, as reported by the NA62 Collaboration [50] and summarized in Ref. [10]. For the channels $K^\pm \rightarrow \pi^\pm a$ and $B \rightarrow K^* a$, the tree-level FCNC contributions originate from the fermion kinetic Lagrangian [33].

In our framework, these contributions are assumed to be absent at the Lagrangian level; hence, the resulting FCNC interactions arise exclusively from field redefinitions and scale proportionally with the PQ charges. As shown in Ref. [33], the decay widths of the pseudoscalar mesons $K^\pm(B)$ into an axion and either a charged pion (K^*) read [33]

$$\begin{aligned} \Gamma(K^\pm \rightarrow \pi^\pm a) &= \frac{m_K^3}{16\pi} \left(1 - \frac{m_\pi^2}{m_K^2}\right)^2 \lambda_{K\pi a}^{1/2} f_0^2(m_a^2) |g_{ads}^V|^2, \\ \Gamma(B \rightarrow K^* a) &= \frac{m_B^3}{16\pi} \lambda_{BK^* a}^{3/2} A_0^2(m_a^2) |g_{asb}^A|^2, \end{aligned} \quad (19)$$

where $\lambda_{Mma} = \left(1 - \frac{(m_a+m)^2}{M^2}\right) \left(1 - \frac{(m_a-m)^2}{M^2}\right)$ and

$$g_{ad_i d_j}^{V,A} = \frac{1}{2 f_a c_3^{\text{eff}}} \Delta_{V,A}^{Dij}, \quad (20)$$

where:

$$\Delta_{V,A}^{Dij} = \Delta_{RR}^{Dij}(d) \pm \Delta_{LL}^{Dij}(q), \quad (21)$$

with

$$\Delta_{LL}^{Fij}(q) = \left(U_L^D x_q U_L^{D\dagger} \right)^{ij}, \quad (22)$$

$$\Delta_{RR}^{Fij}(d) = \left(U_R^D x_d U_R^{D\dagger} \right)^{ij}. \quad (23)$$

In the Eq. (20) we normalize the charges with c_3^{eff} as it is explained in [33]. For $m_a \ll 1$ MeV, the form factor satisfies $f_0(m_a^2) \approx 1$ [51] in $K^\pm \rightarrow \pi^\pm a$ decays. From Ref. [52], one finds $f_0(m_a^2) \approx 0.33$ for $B^\pm \rightarrow K^\pm a$, $f_0(m_a^2) \approx 0.258$ for $B^\pm \rightarrow \pi^\pm a$, and $A_0(m_a^2) \approx 0.374$ for $B^\pm \rightarrow K^* a$.

The limits on the axion couplings and on the decay constant f_a may be extracted from rare semileptonic transitions $M \rightarrow m \bar{\nu} \nu$, with $M = K^\pm, B^\pm$ and $m = \pi^\pm, K^\pm, K^{*\pm}$, and ρ . These bounds are collected in Table 7.1. Figure 2 displays the dependence of f_a on ϵ . For our charge assignment, the contributions to $B^\pm \rightarrow \pi^\pm a$ and $B^\pm \rightarrow K^\pm a$ are highly suppressed, leaving $K^\pm \rightarrow \pi^\pm a$ as the dominant and most constraining channel.

Collaboration	upper bound
N62 Collaboration [50]	$\mathcal{B}(K^+ \rightarrow \pi^+ a) < (9.6.0^{+1.9}_{-1.8}) \times 10^{-11}$
CLEO [53]	$\mathcal{B}(B^\pm \rightarrow \pi^\pm a) < 4.9 \times 10^{-5}$
CLEO [53]	$\mathcal{B}(B^\pm \rightarrow K^\pm a) < 4.9 \times 10^{-5}$
BELLE [54]	$\mathcal{B}(B^\pm \rightarrow \rho^\pm a) < 21.3 \times 10^{-5}$
BELLE [54]	$\mathcal{B}(B^\pm \rightarrow K^{*\pm} a) < 4.0 \times 10^{-5}$

(24)

Table 3. These inequalities come from the window for new physics in the branching ratio uncertainty of the meson decay in a pair $\bar{\nu}\nu$.

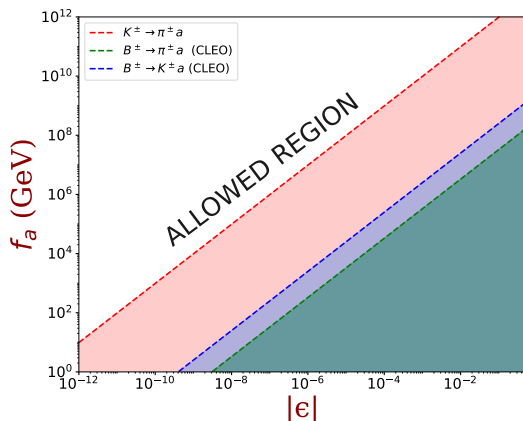


Fig. 2. Allowed regions by lepton decays. For the down-type quarks and charged leptons the non-universal part of the PQ charges just depend on the difference $s_2 - s_1 = N\epsilon/9$, hence the flavor-changing neutral-current couplings (the off diagonal elements) just depend on ϵ .

Astrophysical considerations—including black-hole superradiance and the SN 1987A bounds on the neutron electric dipole moment—further restrict the axion decay constant to the range [10] (see Fig. 2): $0.8 \times 10^6 \text{ GeV} \leq f_a \leq 2.8 \times 10^{17} \text{ GeV}$.

7.2 Constraints on the axion-photon coupling

As shown in Appendix A, the low-energy effective Lagrangian contains the axion-photon interaction

$$\mathcal{L} \supset -\frac{1}{4} g_{a\gamma} a F_{\mu\nu} \tilde{F}^{\mu\nu}, \quad (25)$$

which provides one of the most sensitive experimental probes of axions and axion-like particles (ALPs). The corresponding constraints in the $(m_a, g_{a\gamma})$ plane are summarized in Fig. 3. Below we briefly review the main classes of searches relevant to our parameter space.

Axion searches based on the photon coupling can be grouped into three categories: (i) haloscopes, which target axion dark matter in the Galactic halo; (ii) helioscopes, which search for solar axions; and (iii) purely laboratory experiments based on photon-axion conversion.

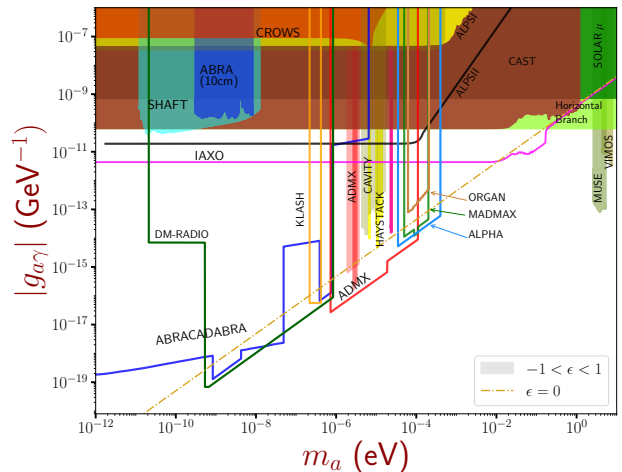


Fig. 3. The excluded parameter space by various experiments corresponds to the colored regions, the dashed-lines correspond to the projected bounds of coming experiments looking for axion signals [55]. The gray region corresponds to the parameter space scanned by our model.

Haloscopes. Haloscope experiments exploit resonant photon-axion conversion in microwave cavities or broadband magnetized detectors. Leading constraints in the μeV range are provided by ADMX [56, 57, 58], which has reached sensitivity to QCD-axion models in the mass window around $m_a \sim \mathcal{O}(1-10)\mu\text{eV}$. Complementary exclusions at nearby masses have been reported by HAYSTAC [59, 60] and by the CAPP collaboration [61, 62, 63]. At higher masses ($m_a \sim 100\mu\text{eV}$), first results from MADMAX further constrain $g_{a\gamma}$, while at ultralow masses ($m_a \lesssim \text{neV}$) broadband searches such as ABRACADABRA set leading limits. Together, these experiments exclude significant portions of parameter space under the assumption that axions constitute the local dark matter density.

Helioscopes. Helioscope searches rely on axion production in the Sun via the Primakoff process and subsequent conversion into x rays in a laboratory magnetic field. The strongest bound to date is provided by CAST,

$$g_{a\gamma} < 5.8 \times 10^{-11} \text{ GeV}^{-1} \quad (95\% \text{ C.L.}), \quad (26)$$

for $m_a \lesssim 0.02\text{eV}$ [64, 65]. The next-generation experiment IAXO is expected to improve this sensitivity by more than one order of magnitude, probing a substantial fraction of the QCD-axion band. These constraints are independent of the cosmological axion abundance.

Laboratory searches. Laboratory-based experiments test photon-axion conversion under controlled conditions, without astrophysical assumptions. Light-shining-through-a-wall experiments such as ALPS-II [66, 67] and OSQAR [68] constrain $g_{a\gamma}$ at low masses, while polarization experiments such as PVLAS [69, 70] probe vacuum birefringence and dichroism induced by ALPs. Although currently less

sensitive than haloscopes or helioscopes in the QCD-axion region, these searches provide model-independent bounds.

Astrophysical constraints. Additional limits arise from stellar energy-loss arguments. Observations of horizontal-branch stars constrain $g_{a\gamma}$ at the level of $g_{a\gamma} \lesssim 6 \times 10^{-11} \text{ GeV}^{-1}$ [71], while solar neutrino data and other indirect probes provide complementary bounds [72, 73, 74]. These constraints are particularly relevant in the sub-eV mass range.

Summary of excluded regions. The combined exclusions from haloscope, helioscope, laboratory, and astrophysical observations are displayed in Fig. 3. The figure shows that present data probe a broad range of masses, from $m_a \sim 10^{-12} \text{ eV}$ up to $m_a \sim 10^{-1} \text{ eV}$, excluding sizeable regions of the $(m_a, g_{a\gamma})$ plane. As discussed below, a nontrivial fraction of our model parameter space overlaps with these experimentally excluded domains.

8 Discussion and conclusions

In this work, we have presented a realization of a flavored Peccei–Quinn symmetry that simultaneously addresses the strong CP problem, the fermion flavor structure, and the origin of neutrino masses within an extended scalar sector. The framework is constructed by enlarging the scalar content of the Standard Model to include four Higgs doublets and two scalar singlets, supplemented by right-handed neutrinos and a vector-like quark. The imposed PQ symmetry governs both the axion dynamics and the Yukawa structure of the model.

We have shown that the PQ charge assignments allow the generation of Hermitian quark mass matrices with five texture zeros, reproducing the observed quark masses, CKM mixing parameters, and CP-violating phase.

Neutrino masses arise through a Type-I seesaw mechanism, where the spontaneous breaking of the PQ symmetry generates Majorana masses for right-handed neutrinos. This mechanism leads to an intrinsic relation between the neutrino mass scale and the axion decay constant, providing a direct link between neutrino physics and axion phenomenology.

The scalar sector exhibits a rich mass spectrum containing multiple CP-even, CP-odd, and charged scalar states. The hierarchical pattern of vacuum expectation values naturally aligns one scalar state with the observed 125 GeV Higgs boson while allowing the presence of additional light and heavy scalars. In particular, the model can accommodate a light CP-even scalar near 95 GeV, potentially connected with diphoton excesses reported in collider searches, while heavier scalar states remain consistent with current LHC bounds and provide promising targets for future experimental exploration.

We have analyzed low-energy and astrophysical constraints arising from flavor-changing neutral currents, rare

meson decays, and axion-photon interactions. The results indicate that viable regions of parameter space exist where all current experimental limits are satisfied. In this context, semileptonic kaon decays provide the most stringent flavor constraints, while astrophysical observations and axion search experiments impose complementary bounds on the axion decay constant and couplings.

An additional appealing feature of the model is the improved naturalness of the Yukawa sector. Most Yukawa couplings in the quark sector are naturally of order unity, while the neutrino sector requires significantly less fine-tuning compared with the Standard Model expectations. This suggests that flavored PQ symmetries may provide a robust mechanism for explaining fermion mass hierarchies.

Overall, our results demonstrate that flavored PQ constructions with multi-Higgs realizations constitute a viable and predictive framework capable of linking axion physics, flavor structures, and neutrino mass generation. Future collider measurements, flavor experiments, and dedicated axion searches will play a crucial role in probing the parameter space of this class of models and testing the proposed connections between these sectors.

Acknowledgments

We thank Professor Roberto Martínez for introducing us to axion physics. This research was partly supported by the “Vicerrectoría de Investigaciones e Interacción Social VIIS de la Universidad de Nariño”, project numbers 3130 and 3595.

A Axion-photon Coupling

At energies well below the Peccei–Quinn (PQ) breaking scale, the axion couplings to gauge fields can be derived by performing suitable chiral field redefinitions [37]. Such transformations leave the classical Lagrangian invariant but induce non-trivial Jacobian factors in the functional measure of the path integral. These anomalous contributions are governed by the divergence of the axial current and generate effective CP-odd interactions between the axion and the gauge-field topological densities. The resulting terms can be written as

$$\begin{aligned} \mathcal{L} \supset & -c_1^{\text{eff}} \frac{\alpha_1}{8\pi} \frac{a}{\Lambda_{\text{PQ}}} B_{\mu\nu} \tilde{B}^{\mu\nu} - c_2^{\text{eff}} \frac{\alpha_2}{8\pi} \frac{a}{\Lambda_{\text{PQ}}} W_{\mu\nu}^3 \tilde{W}^{3\mu\nu} \\ & - c_3^{\text{eff}} \frac{\alpha_3}{8\pi} \frac{a}{f_a} G_{\mu\nu}^a \tilde{G}^{a\mu\nu} \\ = & e^2 C_{\gamma\gamma} \frac{a}{\Lambda_{\text{PQ}}} F_{\mu\nu} \tilde{F}^{\mu\nu} + \frac{e^2 C_{ZZ}}{c_W^2 s_W^2} \frac{a}{\Lambda_{\text{PQ}}} Z_{\mu\nu} \tilde{Z}^{\mu\nu} \\ & + \frac{2e^2 C_{\gamma Z}}{c_W s_W} \frac{a}{\Lambda_{\text{PQ}}} F_{\mu\nu} \tilde{Z}^{\mu\nu} + g_s^2 C_{GG} \frac{a}{\Lambda_{\text{PQ}}} G_{\mu\nu}^a \tilde{G}^{a\mu\nu}. \end{aligned} \quad (27)$$

In the Standard Model, the neutral electroweak gauge fields are related to the physical photon and Z boson

through

$$\begin{aligned} B^\mu &= \cos \theta_W A^\mu - \sin \theta_W Z^\mu, \\ W^{3\mu} &= \sin \theta_W A^\mu + \cos \theta_W Z^\mu, \end{aligned}$$

where A^μ and Z^μ denote the photon and Z -boson fields, respectively. The anomaly coefficients are given by [33]

$$c_1^{\text{eff}} = -\frac{1}{3}\Sigma q + \frac{8}{3}\Sigma u + \frac{2}{3}\Sigma d - \Sigma l + 2\Sigma e, \quad (28)$$

$$c_2^{\text{eff}} = -3\Sigma q - \Sigma l, \quad (29)$$

$$c_3^{\text{eff}} = -2\Sigma q + \Sigma u + \Sigma d - A_Q, \quad (30)$$

where $\Sigma f \equiv f_1 + f_2 + f_3$ represents the sum of the PQ charges over the three fermion families.

For phenomenological applications, it is convenient to introduce

$$\begin{aligned} C_{\gamma\gamma} &= -\frac{1}{32\pi^2} (c_1^{\text{eff}} + c_2^{\text{eff}}), \quad C_{GG} = -\frac{1}{32\pi^2} c_3^{\text{eff}}, \\ C_{ZZ} &= -\frac{1}{32\pi^2} (s_W^4 c_1^{\text{eff}} + c_W^4 c_2^{\text{eff}}), \\ C_{\gamma Z} &= -\frac{1}{32\pi^2} (c_W^2 c_2^{\text{eff}} - s_W^2 c_1^{\text{eff}}). \end{aligned} \quad (31)$$

It is customary to define the effective PQ scale as $\Lambda_{\text{PQ}} = |c_3^{\text{eff}}| f_a$, as well as the ratio

$$\frac{E}{N} = \frac{c_1^{\text{eff}} + c_2^{\text{eff}}}{c_3^{\text{eff}}}. \quad (32)$$

The axion–photon coupling then takes the form [10]

$$g_{a\gamma\gamma} = \frac{4e^2 C_{\gamma\gamma}^{\text{eff}}}{\Lambda_{\text{PQ}}} = -\frac{\alpha}{2\pi f_a} \left(\frac{E}{N} - 2.03 \right), \quad (33)$$

with $\alpha = e^2/(4\pi)$.

Finally, nonperturbative QCD effects associated with the gluon–axion interaction generate a potential for the axion field, which at low energies can be described in terms of axion–pion mixing [75]. The corresponding axion mass is approximately

$$m_a = 5.7(7) \mu\text{eV} \left(\frac{10^{12} \text{ GeV}}{f_a} \right). \quad (34)$$

B Axion decay constant f_a in multi-Higgs models

Consider n complex scalar fields Φ_i (indexed by $i = 1, \dots, n$) which transform under a global $U(1)_{\text{PQ}}$ as

$$\Phi_i \rightarrow e^{ix_i\alpha} \Phi_i, \quad (35)$$

where x_i are the PQ charges of Φ_i (integers or rational numbers) and α is a constant and uniform parameter. Each field develops a vacuum expectation value (VEV):

$$\langle \Phi_i \rangle = \frac{v_i}{\sqrt{2}} > 0. \quad (36)$$

Parametrize fluctuations about the vacuum in polar form (radial + angular decomposition):

$$\Phi_i(x) = \frac{1}{\sqrt{2}} (v_i + \rho_i(x)) e^{iA_i(x)/v_i}, \quad (37)$$

where $\rho_i(x)$ are the radial (massive) modes and $A_i(x)$ are the angular fields (phases). The kinetic part of the scalar Lagrangian contains

$$\mathcal{L}_{\text{kin}} = \sum_i |\partial_\mu \Phi_i|^2 \supset \frac{1}{2} \sum_i (\partial_\mu A_i)(\partial^\mu A_i) + \dots \quad (38)$$

where we omitted radial mode kinetic terms and higher order interactions. To introduce the axion field a we redefined the fields in such a way that

$$\Phi_i \rightarrow e^{\frac{ax_i}{f_a}} \Phi_i \quad (39)$$

That is equivalent to redefining

$$A_i(x) \rightarrow A_i + \frac{x_i v_i}{f_a} a(x) + \dots \quad (40)$$

Inserting this into the kinetic terms (38) yields

$$\begin{aligned} \mathcal{L}_{\text{kin}} &\supset \frac{1}{2} \sum_i \left(\frac{x_i v_i}{f_a} \right)^2 (\partial_\mu a)(\partial^\mu a) + \dots \\ &= \frac{1}{2} \left(\frac{\sum_i x_i^2 v_i^2}{f_a^2} \right) (\partial_\mu a)(\partial^\mu a) + \dots \end{aligned} \quad (41)$$

Requiring the canonical normalization for a real field $\frac{1}{2}(\partial_\mu a)^2$ fixes

$$\boxed{f_a^2 = \sum_{i=1}^n x_i^2 v_i^2} \quad (42)$$

which matches the well-known result [76].

References

1. R. D. Peccei and H. R. Quinn, ‘‘CP Conservation in the Presence of Instantons,’’ *Phys. Rev. Lett.*, vol. 38, pp. 1440–1443, 1977.
2. R. D. Peccei and H. R. Quinn, ‘‘Constraints Imposed by CP Conservation in the Presence of Instantons,’’ *Phys. Rev. D*, vol. 16, pp. 1791–1797, 1977.
3. S. Weinberg, ‘‘A New Light Boson?,’’ *Phys. Rev. Lett.*, vol. 40, p. 223–226, 1978.
4. F. Wilczek, ‘‘Problem of Strong P and T Invariance in the Presence of Instantons,’’ *Phys. Rev. Lett.*, vol. 40, p. 279–282, 1978.
5. J. E. Kim, ‘‘Weak Interaction Singlet and Strong CP Invariance,’’ *Phys. Rev. Lett.*, vol. 43, p. 103, 1979.
6. M. A. Shifman, A. I. Vainshtein, and V. I. Zakharov, ‘‘Can Confinement Ensure Natural CP Invariance of Strong Interactions?,’’ *Nucl. Phys. B*, vol. 166, pp. 493–506, 1980.
7. A. R. Zhitnitsky, ‘‘On Possible Suppression of the Axion Hadron Interactions. (In Russian),’’ *Sov. J. Nucl. Phys.*, vol. 31, p. 260, 1980.

8. M. Dine, W. Fischler, and M. Srednicki, “A Simple Solution to the Strong CP Problem with a Harmless Axion,” *Phys. Lett. B*, vol. 104, pp. 199–202, 1981.
9. J. E. Kim and G. Carosi, “Axions and the Strong CP Problem,” *Rev. Mod. Phys.*, vol. 82, p. 557–602, 2010.
10. L. Di Luzio, M. Giannotti, E. Nardi, and L. Visinelli, “The landscape of QCD axion models,” *Phys. Rept.*, vol. 870, pp. 1–117, 2020.
11. L. Calibbi, F. Goertz, D. Redigolo, R. Ziegler, and J. Zupan, “Minimal axion model from flavor,” *Phys. Rev. D*, vol. 95, no. 9, p. 095009, 2017.
12. F. Björkeröth, E. J. Chun, and S. F. King, “Flavourful Axion Phenomenology,” *JHEP*, vol. 08, p. 117, 2018.
13. F. Björkeröth, L. Di Luzio, F. Mescia, and E. Nardi, “ $U(1)$ flavour symmetries as Peccei-Quinn symmetries,” *JHEP*, vol. 02, p. 133, 2019.
14. L. Di Luzio, E. Nardi, and P. Panci, “Accidental Peccei-Quinn symmetries from discrete flavour symmetries,” *Phys. Rev. D*, vol. 96, no. 7, p. 075003, 2017.
15. R. Ziegler, “Flavored Peccei-Quinn symmetry,” *Lect. Notes Phys.*, vol. 938, p. 391–422, 2018.
16. A. N. Author, “ ν DFSZ—A Neutrino-Flavored DFSZ Axion Model,” *Journal of High Energy Physics*, vol. 2025, p. 123, 2025. submitted; placeholder.
17. ATLAS and C. Collaborations, “Combined Measurement of the Higgs boson decay $h \rightarrow Z\gamma$ in pp collisions at $\sqrt{s} = 13$ TeV,” *JHEP*, vol. 05, p. 123, 2024. combined result.
18. C. Collaboration, “Search for high-mass diphoton resonances in proton–proton collisions at $\sqrt{s} = 13$ TeV,” *Phys. Lett. B*, vol. 820, p. 136521, 2024.
19. A. Collaboration, “Search for low-mass diphoton resonances in boosted topologies with the ATLAS detector,” *Phys. Rev. D*, vol. 100, no. 5, p. 052005, 2024.
20. A. Collaboration, “Search for heavy resonances decaying into $Z\gamma$ in proton–proton collisions at $\sqrt{s} = 13$ TeV,” *Eur. Phys. J. C*, vol. 83, no. 7, p. 577, 2023.
21. C. Collaboration, “Search for resonances in Zh final states at $\sqrt{s} = 13$ TeV,” *JHEP*, vol. 08, p. 045, 2025.
22. R. Verma, “Exploring the predictability of symmetric texture zeros in quark mass matrices,” *Phys. Rev. D*, vol. 96, no. 9, p. 093010, 2017.
23. Z.-z. Xing, “Flavor structures of charged fermions and massive neutrinos,” *Phys. Rept.*, vol. 854, pp. 1–147, 2020.
24. H. Fritzsch and Z.-z. Xing, “Mass and flavor mixing schemes of quarks and leptons,” *Prog. Part. Nucl. Phys.*, vol. 45, pp. 1–81, 2000.
25. B. R. Desai and A. R. Vaucher, “Quark mass matrices with four and five texture zeroes, and the CKM matrix, in terms of mass eigenvalues,” *Phys. Rev. D*, vol. 63, p. 113001, 2001.
26. P. O. Ludl and W. Grimus, “A complete survey of texture zeros in general and symmetric quark mass matrices,” *Phys. Lett. B*, vol. 744, pp. 38–42, 2015.
27. W. A. Ponce, J. D. Gómez, and R. H. Benavides, “Five texture zeros and CP violation for the standard model quark mass matrices,” *Phys. Rev. D*, vol. 87, no. 5, p. 053016, 2013.
28. Y. Giraldo, “Texture Zeros and WB Transformations in the Quark Sector of the Standard Model,” *Phys. Rev. D*, vol. 86, p. 093021, 2012.
29. Y. Giraldo and E. Rojas, “CKM mixings from mass matrices with five texture zeros,” *Phys. Rev. D*, vol. 104, no. 7, p. 075009, 2021.
30. Y. Giraldo and E. Rojas, “Five Non-Fritzsch Texture Zeros for Quarks Mass Matrices in the Standard Model,” in *38th International Symposium on Physics in Collision*, 11 2018.
31. G. C. Branco, L. Lavoura, and F. Mota, “Nearest Neighbor Interactions and the Physical Content of Fritzsch Mass Matrices,” *Phys. Rev. D*, vol. 39, p. 3443, 1989.
32. G. C. Branco, D. Emmanuel-Costa, and R. Gonzalez Felipe, “Texture zeros and weak basis transformations,” *Phys. Lett. B*, vol. 477, pp. 147–155, 2000.
33. Y. Giraldo, R. Martinez, E. Rojas, and J. C. Salazar, “Flavored axions and the flavor problem,” *Eur. Phys. J. C*, vol. 82, no. 12, p. 1131, 2022.
34. Y. A. Garnica, S. F. Mantilla, R. Martinez, and H. Vargas, “From Peccei Quinn symmetry to mass hierarchy problem,” *J. Phys. G*, vol. 48, no. 9, p. 095002, 2021.
35. A. Ringwald and K. Saikawa, “Axion dark matter in the post-inflationary Peccei-Quinn symmetry breaking scenario,” *Phys. Rev. D*, vol. 93, no. 8, p. 085031, 2016. [Addendum: Phys.Rev.D 94, 049908 (2016)].
36. I. Brivio, M. B. Gavela, L. Merlo, K. Mimasu, J. M. No, R. del Rey, and V. Sanz, “ALPs Effective Field Theory and Collider Signatures,” *Eur. Phys. J. C*, vol. 77, no. 8, p. 572, 2017.
37. Y. Giraldo, R. Martínez, E. Rojas, and J. C. Salazar, “A minimal axion model for mass matrices with five texture-zeros,” 4 2023.
38. A. E. Cárcamo Hernández, C. Espinoza, J. C. Gómez-Izquierdo, J. Marchant González, and M. Mondragón, “Phenomenology of extended multiHiggs doublet models with S_4 family symmetry,” *Eur. Phys. J. C*, vol. 84, no. 11, p. 1239, 2024.
39. J. A. Aguilar-Saavedra, H. B. Câmara, F. R. Joaquim, and J. F. Seabra, “Confronting the 95 GeV excesses within the $U(1)$ -extended next-to-minimal 2HDM,” *Phys. Rev. D*, vol. 108, no. 7, p. 075020, 2023.
40. Z.-f. Ge, F.-Y. Niu, and J.-L. Yang, “The origin of the 95 GeV excess in the flavor-dependent $U(1)_X$ model,” *Eur. Phys. J. C*, vol. 84, no. 5, p. 548, 2024.
41. S. Baek, P. Ko, Y. Omura, and C. Yu, “96 GeV scalar boson in the 2HDM with $U(1)_H$ gauge symmetry,” *Eur. Phys. J. C*, vol. 85, no. 8, p. 908, 2025.
42. R. Benbrik, M. Boukidi, K. Kahime, S. Moretti, L. Rahili, and B. Taki, “Interpreting the 650 GeV and 95 GeV Higgs Anomalies in the N2HDM,” 10 2025.
43. N. Krishnan, G. Arcadi, G. Busoni, and D. Cabo-Almeida, “Searching for a New (Pseudo)Scalar at 95 GeV,” *PoS*, vol. QCHSC24, p. 270, 2025.
44. A. Hmissou, S. Moretti, and L. Rahili, “Investigating the 95 GeV Higgs boson excesses within the type-I (1+2)HDM,” *Phys. Rev. D*, vol. 113, no. 1, p. 015024, 2026.
45. G. Arcadi and A. Djouadi, “Interpreting the current Higgs excesses at the LHC in the 2HD+a framework,” 12 2025.
46. Y. Dong, M. Ruan, K. Wang, H. Yang, and J. Zhu, “Particle-level transformers for 95 GeV Higgs boson searches at future e^+e^- Higgs factories,” 10 2025.
47. A. M. Coutinho, A. Karan, V. Miralles, and A. Pich, “Light scalars within the CP -conserving Aligned-two-Higgs-doublet model,” *JHEP*, vol. 02, p. 057, 2025.
48. A. Khanna, S. Moretti, and A. Sarkar, “Explaining 650 GeV and 95 GeV Anomalies in the 2-Higgs Doublet Model Type-I,” 9 2025.
49. A. Bhatnagar, D. Croon, and P. Schicho, “Interpreting the 95 GeV resonance in the Two Higgs Doublet Model: Implications for the Electroweak Phase Transition,” 6 2025.

50. R. Fiorenza and NA62 Collaboration, “A new measurement of $\mathcal{B}(K^+ \rightarrow \pi^+ \nu \bar{\nu})$ at the NA62 experiment.” Talk presented at the La Thuile Conference on Results and Perspectives in Particle Physics.
51. N. Carrasco, P. Lami, V. Lubicz, L. Riggio, S. Simula, and C. Tarantino, “ $K \rightarrow \pi$ semileptonic form factors with $N_f = 2 + 1 + 1$ twisted mass fermions,” *Phys. Rev. D*, vol. 93, no. 11, p. 114512, 2016.
52. P. Ball and R. Zwicky, “New results on $B \rightarrow \pi, K, \eta$ decay formfactors from light-cone sum rules,” *Phys. Rev. D*, vol. 71, p. 014015, 2005.
53. R. Ammar *et al.*, “Search for the familon via $B^{+-} \rightarrow \pi^+ X^0, B^{+-} \rightarrow K^+ X^0$, and $B^0 \rightarrow K^0(S) X^0$ decays,” *Phys. Rev. Lett.*, vol. 87, p. 271801, 2001.
54. O. Lutz *et al.*, “Search for $B \rightarrow h^{(*)} \nu \bar{\nu}$ with the full Belle $\Upsilon(4S)$ data sample,” *Phys. Rev. D*, vol. 87, no. 11, p. 111103, 2013.
55. C. O’Hare, “cajohare/axionlimits: Axionlimits.” <https://cajohare.github.io/AxionLimits/>, July 2020.
56. C. Bartram *et al.*, “Search for Invisible Axion Dark Matter in the 3.3–4.2 μeV Mass Range,” *Phys. Rev. Lett.*, vol. 127, no. 26, p. 261803, 2021.
57. T. Braine *et al.*, “Extended Search for the Invisible Axion with the Axion Dark Matter Experiment,” *Phys. Rev. Lett.*, vol. 124, no. 10, p. 101303, 2020.
58. C. Bartram *et al.*, “Axion dark matter experiment: Run 1B analysis details,” *Phys. Rev. D*, vol. 103, no. 3, p. 032002, 2021.
59. K. M. Backes *et al.*, “A quantum-enhanced search for dark matter axions,” *Nature*, vol. 590, no. 7845, pp. 238–242, 2021.
60. L. Zhong *et al.*, “Results from phase 1 of the HAYSTAC microwave cavity axion experiment,” *Phys. Rev. D*, vol. 97, no. 9, p. 092001, 2018.
61. S. Lee, S. Ahn, J. Choi, B. R. Ko, and Y. K. Semertzidis, “Axion Dark Matter Search around 6.7 μeV ,” *Phys. Rev. Lett.*, vol. 124, no. 10, p. 101802, 2020.
62. J. Jeong, S. Youn, S. Bae, J. Kim, T. Seong, J. E. Kim, and Y. K. Semertzidis, “Search for Invisible Axion Dark Matter with a Multiple-Cell Haloscope,” *Phys. Rev. Lett.*, vol. 125, no. 22, p. 221302, 2020.
63. O. Kwon *et al.*, “First Results from an Axion Haloscope at CAPP around 10.7 μeV ,” *Phys. Rev. Lett.*, vol. 126, no. 19, p. 191802, 2021.
64. V. Anastassopoulos *et al.*, “New CAST Limit on the Axion-Photon Interaction,” *Nature Phys.*, vol. 13, pp. 584–590, 2017.
65. E. Arik *et al.*, “Probing ev-scale axions with cast,” *Phys. Rev. Lett.*, vol. 100, p. 021802, 2008.
66. R. Bähre *et al.*, “Any light particle search II — Technical Design Report,” *JINST*, vol. 8, p. T09001, 2013.
67. B. Döbrich and A. Ringwald, “The ALPS II experiment: status and prospects,” *Symmetry*, vol. 12, no. 9, p. 1570, 2020.
68. R. Ballou *et al.*, “Search for weakly interacting sub-eV particles with the OSQAR laser-based experiment: results and perspectives,” *Phys. Rev. D*, vol. 92, no. 9, p. 092002, 2015.
69. E. Zavattini *et al.*, “Experimental observation of optical rotation generated in vacuum by a magnetic field,” *Phys. Rev. Lett.*, vol. 96, p. 110406, 2006.
70. E. Zavattini *et al.*, “New PVLAS results and limits on magnetically induced optical rotation and ellipticity in vacuum,” *Phys. Rev. D*, vol. 77, p. 032006, 2008.
71. A. Ayala, I. Domínguez, M. Giannotti, A. Mirizzi, and O. Straniero, “Revisiting the bound on axion-photon coupling from Globular Clusters,” *Phys. Rev. Lett.*, vol. 113, no. 19, p. 191302, 2014.
72. P. Gondolo and G. G. Raffelt, “Solar neutrino limit on axions and keV-mass bosons,” *Phys. Rev. D*, vol. 79, p. 107301, 2009.
73. M. Regis, M. Taoso, D. Vaz, J. Brinckmann, S. L. Zoutendijk, N. F. Bouché, and M. Steinmetz, “Searching for light in the darkness: Bounds on ALP dark matter with the optical MUSE-faint survey,” *Phys. Lett. B*, vol. 814, p. 136075, 2021.
74. D. Grin, G. Covone, J.-P. Kneib, M. Kamionkowski, A. Blain, and E. Jullo, “A Telescope Search for Decaying Relic Axions,” *Phys. Rev. D*, vol. 75, p. 105018, 2007.
75. G. Grilli di Cortona, E. Hardy, J. Pardo Vega, and G. Villadoro, “The QCD axion, precisely,” *JHEP*, vol. 01, p. 034, 2016.
76. M. Srednicki, “Axion Couplings to Matter. 1. CP Conserving Parts,” *Nucl. Phys. B*, vol. 260, pp. 689–700, 1985.